VIBRATION ANALYSIS

OF

HAMMER-SHANK SYSTEM

CBS TECHNOLOGY CENTER

VIBRATION ANALYSIS

OF

HAMMER-SHANK SYSTEM

Prepared by: Hideo Suzuki

April 7, 1983

CBS Technology Center
227 High Ridge Road
Stamford, CT 06905

ABSTRACT

The transient motion of the hammer-shank system is mathematically analyzed using a modified form of the Myklestad method. The hammer is modeled as a mass-spring system with a non-linear spring coefficient. The shank is divided into thirteen elements, where each element is assumed to have a uniform cross-section. The effect of the shank stiffness, the hammer velocity, and the initial deformation of the shank on the force-time pattern applied by the hammer to an ideally rigid string is investigated. The results show that the shank suffers a significantly large deformation during the hammer-string contact period. It is also shown that the force-time pattern changes significantly when a non-zero initial deformation of the shank is introduced. Some of the theoretical results are compared with experimental results.

LIST OF SYMBOLS

B_j Bending stiffness of jth element ($=E_s \cdot I_j$)

E_s Young's modulus of the shank

L Superscript indicating a variable of the left-hand side of the lumped mass

M_h Hammer mass

$M_j^{L,R}$ Left- and right-hand side moments, respectively

N Highest element number of the shank

R Superscript indicating a variable of the right-hand side of the lumped mass

S_h Hammer stiffness

$V_j^{L,R}$ Left- and right-hand side sheer forces, respectively

a Width of rectangular shank element

b Height of the rectangular shank element

j Element number

l_j Length of the jth element

m_j Mass of the jth element

r Radius of circular shank element

$v_j^{L,R}$ Left- and right-hand side velocities, respectively

y_h Deformation of the hammer spring

$y_j^{L,R}$ Left- and right-hand side displacements, respectively

$j^{L,R}$ Left- and right-hand side accelerations, respectively

$O_j^{L,R}$ Left- and right-hand side slope of the lumped mass, repectively

ρ_s Mass density of the shank

ΔT Time increment

INTRODUCTION

The hammers, strings, and soundboard are the main contributors to the total sound quality of the piano. The enormous number of studies that have been devoted to these parts is solid proof of this fact. On the other hand, some parts such as the rim, the plate, and the key action are believed to have secondary effects on the total quality. Nonetheless, the effects of these parts should not be ignored when considering the improvement of the total system. The shank of the piano hammer seems to be one of those parts to which more attention should be paid. It is empirically known that the tonal quality changes when the shanks are replaced from one kind of wood to another. This seems reasonable if the motion of the hammer at the time of contact with the string is considered. The hammer has a speed of several meters per second when the key is hit very hard. This hammer is bounced back by the string within a very short period of time (millisecond order). It is not difficult to believe that the shank may suffer some amount of deformation, or some vibratory motion, which may cause some difference in the vibration of the string.

Another interesting aspect of the shank is that the "hammer-shank" system provide a way to explain the difference of the sound qualities when a single key is excited with different "touches". The hammer-shank system is not a single-degree-of-freedom system, and therefore, the "hammer velocity" is not sufficient to describe the initial

condition. If there is any difference between the initial motions of the shank for different touches, this might cause different excitations of the string.

Many studies have been conducted on the interaction of the hammer and the string [1] - [13]. But none of them includes the motion of the shank in the analysis of the hammer-string interaction. In our mathematical model, the deformation and the velocity of the shank as well as the velocity of the hammer will be taken into account as the initial condition. The effect of these shank parameters will be discussed by investigating the force-time pattern applied by the hammer to an ideally rigid string. A modified version of the Myklestad method is used for the analysis of the hammer-shank system. Measurement of the force-time pattern will also be discussed for comparison with results obtained from the analysis.

I. MODEL OF HAMMER-SHANK SYSTEM

A model used for the present study is shown in Fig. 1. For a complete analysis of the hammer-string interaction, the string also must be represented by a mathematical model and combined with the hammer-shank model. In the present study, however, the string is assumed to be infinitely rigid. This assumption is employed because the

number of variables in the analysis can be significantly reduced, and still the model is expected to give enough information concerning the effect of the shank.

The hammer is simulated by a mass-spring system with mass M_h and stiffness S_h. The significant difference of this model from previous studies is that the stiffness S_h has quite a high order of nonlinearity. The hammer mass and the stiffness used for the calculations are $M_h = 10$ gram and $S_h = 1.8 \times 10^{10} y_h^3$ dyne/cm, where y_h is the deformation of the hammer. (The derivation of M_h and S_h from measured data will be discussed in another paper.)

The shank is simply supported at one end and firmly joined to the hammer at the other end. Also the shank is divided into thirteen elements, where each element is uniform along its length. The dimensions of the shank element are shown in Table I. Furthermore, each element is expressed by a system consisting of a lumped-mass and a massless elastic beam as shown in Fig. 2. The lumped mass m_j is given as the average of masses of elements (j-1) and (j) in Fig. 1. The mass m_1 is one-half of the mass of the element 1, and m_{N+1} =10.1 gram is the sum of the one-half of the mass of the element N and the hammer mass M_h. For convenience, the values of mass m_j, j = 1, 2, ..., N are also shown in Table I, where ρ_h = 0.72 gram/cm^3 is assumed as the density of the maple wood normally used for the shank.

II. MATHEMATICAL DISCUSSION

The method given by N. O. Myklestad [14] was suggested as a technique for numerical solution of the natural frequencies and principal modes of a non-uniform beam (steady-state problem). This formula must be modified to a suitable form for the analysis of the transient motion of the hammer-shank system. The derivation of this formula is shown below.

The relationship between the state vectors of the left and right hand sides of the mass m_j in Fig. 2 is given by [15]:

$$\begin{Bmatrix} V \\ M \\ \theta \\ y \end{Bmatrix}^R = \begin{bmatrix} 1 & 0 & 0 & -m_j \frac{d^2}{dt^2} \\ 0 & 1 & 0 & 0 \\ 0 & 0 & 1 & 0 \\ 0 & 0 & 0 & 1 \end{bmatrix} \begin{Bmatrix} V \\ M \\ \theta \\ y \end{Bmatrix}^L_j \tag{1}$$

A similar relationship between the state vectors of the left and right hand side of the massless beam is obtained such as:

$$\begin{Bmatrix} V \\ M \\ \theta \\ y \end{Bmatrix}^L_{j+1} = \begin{bmatrix} 1 & 0 & 0 & 0 \\ \ell_j & 1 & 0 & 0 \\ \frac{\ell_j^2}{2B_j} & \frac{\ell_j}{B_j} & 1 & 0 \\ \frac{\ell_j^3}{6B_j} & \frac{\ell_j^2}{2B_j} & \ell_j & 1 \end{bmatrix} \begin{Bmatrix} V \\ M \\ \theta \\ y \end{Bmatrix}^R_j \tag{2}$$

Substituting Eq. (1) into Eq. (2), we have:

$$\begin{Bmatrix} V \\ M \\ \theta \\ y \end{Bmatrix}_{j+1}^{L} = \begin{bmatrix} 1 & 0 & 0 & -m_j \frac{d^2}{dt^2} \\ \ell_j & 1 & 0 & -m_j \ell_j \frac{d^2}{dt^2} \\ \frac{\ell_j^2}{2B_j} & \frac{\ell_j}{B_j} & 1 & -m_j \frac{\ell_j^2}{2B_j} \frac{d^2}{dt^2} \\ \frac{\ell_j^3}{6B_j} & \frac{\ell_j^2}{2B_j} & \ell_j & 1 - m_j \frac{\ell_j^3}{6B_j} \frac{d^2}{dt^2} \end{bmatrix} \begin{Bmatrix} V \\ M \\ \theta \\ y \end{Bmatrix}_{j}^{L} \qquad (3)$$

Eq. (3) can be rewritten as:

$$\begin{bmatrix} 1 & 0 & 0 & -m_j & -1 & 0 & 0 & 0 \\ \ell_j & 1 & 0 & -m_j \ell_j & 0 & -1 & 0 & 0 \\ \frac{\ell_j^2}{2B_j} & \frac{\ell_j}{B_j} & 1 & -m_j \frac{\ell_j^2}{2B_j} & 0 & 0 & -1 & 0 \\ \frac{\ell_j^3}{6B_j} & \frac{\ell_j^2}{2B_j} & \ell_j & -m_j \frac{\ell_j^3}{6B_j} & 0 & 0 & 0 & 0 \end{bmatrix} \begin{Bmatrix} V_j \\ M_j \\ \theta_j \\ \alpha_j \\ V_{j+1} \\ M_{j+1} \\ \theta_{j+1} \\ \alpha_{j+1} \end{Bmatrix}^{L} = \begin{Bmatrix} 0 \\ 0 \\ 0 \\ y_{j+1} - y_j \end{Bmatrix}^{L} \qquad (4)$$

where $\alpha_j = d^2y_j/dt^2$ was used. This is the modified form of Myklestad's formula used in our study, which supplies a set of (Nx4) simultaneous equations (j = 1, 2, ..., N).

Four more equations are needed for the solution of the system since we have (N+1)x4 unknowns. These are given by the boundary conditions at the left and right hand side of the shank, such as:

$$\left.\begin{aligned} \alpha_1^L &= 0 \quad (\text{with } y_1 \equiv 0) \\ M_1^L &= 0 \end{aligned}\right\} \tag{5}$$

and

$$\left.\begin{aligned} V_{N+1}^L &= m_{N+1} \cdot \alpha_{N+1}^L + S_h y_{N+1}^L \\ M_{N+1}^L &= 0 \end{aligned}\right\} \tag{6}$$

Combining Eq. (4), (5), and (6), we have a set of (N+1)x4 equations.

$$
\begin{bmatrix}
0 & 0 & 0 & 1 & 0 & 0 & 0 & 0 & 0 & \cdot \\
0 & 1 & 0 & 0 & 0 & 0 & 0 & 0 & 0 & \cdot \\
1 & 0 & 0 & -m_1 & -1 & 0 & 0 & 0 & 0 & \cdot \\
\ell_1 & 1 & 0 & -m_1\ell_1 & 0 & -1 & 0 & 0 & 0 & \cdot \\
\frac{\ell_1^2}{2B_1} & \frac{\ell_1^2}{B_1} & 1 & -m_1\frac{\ell_1^2}{2B_1} & 0 & 0 & -1 & 0 & 0 & \cdot \\
\frac{\ell_1^3}{6B_1} & \frac{\ell_1^2}{2B_1} & \ell_1 & -m_1\frac{\ell_1^3}{6B} & 0 & 0 & 0 & 0 & 0 & \cdot \\
0 & 0 & 0 & 0 & 1 & 0 & 0 & -m_2 & -1 & \cdot \\
0 & 0 & 0 & 0 & \ell_2 & 1 & 0 & -m_2\ell_2 & 0 & \cdot \\
0 & 0 & 0 & 0 & \frac{\ell_2^2}{2B_2} & \frac{\ell_2}{B_2} & 1 & -m_2\frac{\ell_2^2}{2B_2} & 0 & \cdot \\
\approx & \cdot & \cdot & \cdot & \cdot & \cdot & \cdot & \cdot & \cdot & \cdot \\
 & & & & \cdot & -m_{N-1} & \frac{\ell_{N-1}^3}{6B_{N-1}} & 0 & 0 & 0 \\
 & & & & \cdot & 0 & 1 & 0 & 0 & -m_N \\
 & & & & \cdot & 0 & \ell_N & 1 & 0 & -m_N\ell_N \\
 & & & & \cdot & 0 & \frac{\ell_N^2}{2B_N} & \frac{\ell_N}{B_N} & 1 & -m_N\frac{\ell_N^2}{2B_N} \\
 & & & & \cdot & 0 & \frac{\ell_N^3}{6B_N} & \frac{\ell_N^2}{2B_N} & \ell_N & -m_N\frac{\ell_N^3}{6B_N} \\
 & & & & \cdot & 0 & 0 & 0 & 0 & 0 \\
 & & & & \cdot & 0 & 6 & 0 & 0 & 0
\end{bmatrix}
\begin{pmatrix} V_1 \\ M_1 \\ \theta_1 \\ \alpha_1 \\ V_2 \\ M_2 \\ \theta_2 \\ \alpha_2 \\ \vdots \\ \approx \\ M_N \\ \theta_N \\ \alpha_N \\ V_{N+1} \\ M_{N+1} \\ \theta_{N+1} \\ \alpha_{N+1} \end{pmatrix}
=
\begin{pmatrix} 0 \\ 0 \\ 0 \\ 0 \\ 0 \\ y_2 - y_1 \\ 0 \\ 0 \\ \vdots \\ \approx \\ y_N - y_{N-1} \\ 0 \\ 0 \\ 0 \\ y_{N+1} - y_N \\ y_{N+1} \\ 0 \end{pmatrix}
\qquad (7)
$$

This is the nonlinear system equation valid at any instantaneous time.

Eq. (7) shows that if we give the initial displacement vector $y(t=0)_j$, the acceleration vector $(t=0)_j$ is determined. Then, after a short period of time (ΔT), the displacement vector is approximated using the formula:

$$\{y(\Delta T)\}_j = \{v(0)\}_j \Delta T + \{\alpha(0)\}_j (\Delta T)^2/2 \qquad (8)$$

Here, we are utilizing the two initial conditions, i.e., the displacement vector $\{y(t)\}_j$ and the velocity vector $\{v(t)\}_j$ at t=0. The velocity vector at $t = \Delta T$ is also approximated by

$$\{v(\Delta T)\}_j = \{v(0)\}_j + \{\alpha(0)\}_j \Delta T \qquad (9)$$

By repeating the same process, we can calculate the displacement vector at any time (if the solution does not diverge). It is convenient that the matrix of Eq. (7) does not contain any time variant term. Once the inverse of the left hand side matrix is calculated, the solution of Eq. (7) is simply obtained by the multiplication of this inverse matrix and the right hand side vector.

$$\{y(\Delta T)\}_j = \{y(0)\}_j + \{v(0)\}_j \Delta t$$
$$\{v(\Delta t)\}_j = \{v(0)\}_j + \{a(0)\}_j \Delta t$$

III. RESULTS AND DISCUSSION

The frequency spectrum of the vibration of the string is dependent on the sharpness of the force applied by the hammer at the time of contact. If the hammer stiffness is large, the contact time becomes small, and consequently, the frequency spectrum pattern of the string vibration becomes wide, producing a brighter sound. Thus, the evaluation of the force-time pattern applied by the hammer to the string (assumed to be infinitely rigid in our model) is most important investigating the effect of the hammer-shank system on the quality of the piano sound. The effects of the shank stiffness, the initial deformation of the shank, and the hammer velocity on this force-time pattern are discussed in this section.

3.1 Effect of Shank Stiffness

Table II shows the standard values used to calculate the force-time pattern. The parameters of the hammer were determined by measureing the bass hammer. The Young's modulus $E_s = 10^{11}$ dyne/cm^2 and the density of the shank $\rho_s = 0.72$ gram/cm^3 were used as representative values for maple. The initial velocity of the hammer-shank system is represented by the speed of the hammer at the beginning of the contact. The hammer velocity is 3 m/sec except where otherwise stated. This corresponds to the speed of the hammer when the key is hit

very hard. The velocity profile of the shank is always assumed to be linear (i.e., the velocity at each joint is proportional to the distance from the pivot). The initial deformation of the shank is assumed to be zero except where otherwise stated.

The force-time pattern calculated using these standard values is shown by the line (a) in Fig. 3. The peak force (i.e., corresponds to the peak deformation of the hammer) occurs at t = 0.7 msec, and the shape of the force-time pattern is approximately symmetric. The symmetry of the pulse is considered to be the result of (1) the assumption that the hammer has no damping, and (2) the relatively small contribution of the shank motion to the motion of the hammer. Figure 4 shows the deformation of the shank at different times during the hammer-string contact period. At t = 0, the deformation of the shank is zero from the assumption. Until t = 0.4 msec, the shank does not show much deformation. However, the shank suffers large deformation at around t = 1.1 msec. This is because the shank still tends to move upward even after the hammer has already started moving to the opposite direction. The largest deformation is seen around element #7, and its magnitude is approximately 0.75 mm.

In order to see the effect of the shank stiffness, the Young's modulus of the shank was increased to 10^{12} dyne/cm^2. The force time pattern and the shank deformation are shown by the line (b) in Fig. 3 and by the several curves in Fig. 5, respecively. The difference between the two curves in Fig. 3 is very small. Both the peak level and the width

of the pulse are slightly increased for the stiffer shank. Figure 5 shows that the deformation of the shank is almost negligible in case of an ideally stiff shank. The larger peaks and the wider pulse can be considered as the result of the increased effective mass of the hammer. Since the hammer-shank system is almost a rigid body, a large portion of the shank mass may work as a part of the hammer mass. The observation of the motion of the hammer-shank system using a high-speed camera shows the deformation of approximately 0.4 mm (0 to peak) for a slower hammer speed, confirming the present result obtained by our model.

3.2 Effect of Initial Shank Deformation

The hammer is accelerated from its rest position to a speed of 3 m/sec approximately in 20 msec. Considering this large acceleration, it might be assumed that the shank is already deformed when the hammer hits the string. It is not easily investigated how much and to which direction the shank is deformed at $t = 0$. If the shank is pushed upward with a constant acceleration, the hammer may be deformed to the positive direction (i.e., the center portion of the shank may have a positive displacement at $t = 0$). On the other hand, if the hammer-shank system is accelerated drastically at the beginning and flies almost freely after that, there is a chance that the shank may be deformed to the negative direction at $t = 0$, due to the natural vibration of the system. (A good example of this is a golf club. Right before the club head hits

the golf ball, the shaft is deformed to the negative direction.)

Force-time patterns for the positive and negative initial deformations are shown by the curves (a) and (b) in Fig. 6, respectively. The deformation curves are shown in Figs. 7 and 8 for the positive and negative initial deformations, respectively. The shape of the deformation was chosen from the last curve in Fig. 4 (t = 1.45 msec), since this might show a natural mode of the system. The maximum deformation was $\pm$0.5 mm at j=7. Figure 6 shows that the initial deformation of the shank has a significant effect on the force-time pattern. If the shank is deformed to the positive direction, the peak level is higher and the pulse width is narrower. The force-time pattern for the negative initial deformation shows a slight asymmetry. The motion of the shank for these cases is very complex during the contact period. Figure 7 indicates some oscillatory motion of the shank even though the shank does not show a negative deformation. Considering these large deformations of the shank, the effect of the shank on the motion of the hammer still seems minor. If a hammer with smaller mass had been used in our model, the result might have been different.

3.3 Effect of Hammer Velocity

The evaluation of the force-time patterns in Fig. 6 is not easy since the peak levels and pulse widths are both different. For a better comparison, a force-time pattern was calculated with an increased hammer velocity for the case of the negative initial deformation. With V_h = 3.29 m/sec, the peak level of the force-time pattern equals that of the positive shank deformation with V_h = 3 m/sec. These two curves are compared in Fig. 9. The line (b) shows the result of the negative shank deformation with V_h = 3.29 m/sec. The line (a) is the same as the line (a)in Fig. 6. The shapes are quite similar to each other, but the force-time pattern with the negative shank deformation has larger width. Consequently, if it is possible to listen to these signals through a high fidelity reproducing system, the timber may be slightly different for those two signals. Relatively speaking, the narrower pulse has larger high frequency components. Therefore, the signal shown by the line (b) in Fig. 9 should sound brighter than the other. This result indicates that if the initial shank deformation is controllable by the touch of the player, the timber may change due to the difference of the touch, even if the loudness change is unnoticeable.

3.4 Measurement of Force-Time Pattern

The force-time pattern of a hammer for key #3 (which has slightly different characteristics from the mathematical model) were measured using a key-action model. The hammer hits a string-like tip which is made of steel. This is fixed to a piezo-electric force transducer, which is attached to a very rigid arm hanging over one hammer. The transducer picks up the transient force applied by the hammer to the string-like tip.

The first measurement was conducted on the hammer with two kinds of shank material. Firstly, the force-time pattern of the hammer with a wood shank was measured. Then, the shank was replaced by a carbon fiber tube (its stiffness is approximately twice that of the wood shank) and the force-time pattern was again measured. The results are shown by the lines (a) and (b) in Fig. 10, respectively.

The force-time pattern with the carbon shank is wider than that of the wood shank showing an agreement with the result of the mathematical model (Fig. 3).

The second measurement was intended to see if there is any difference between the force-time patterns with different touches. The hammer-shank system was excited in three different ways: (1) the key is accelerated through the whole key excursion, (2) the key was accelerated only during the first half of the excursion, and (3) the key was accelerated only during the latter half of the excursion. In case (1), the hammer was accelerated more slowly for a longer period of time

than in cases (2) and (3). The difference between cases (2) and (3) is the timing of the acceleration. For all three cases, it was attempted to hold the peak values of the force-time patterns the same. It should be noted that in cases (2) and (3) the key had to be hit much harder than in case (1) to produce the same peak value of the force. Unfortunately, the force-time patterns for these cases were too close to identify any differences. This indicates that the initial deformation of the shank is much smaller than 0.5 mm, the value used in Sec. 3.2, and 3.3.

Judging from the result of the second experiment, the effect of the touch turned out to be negligible, or at least it was not apparent from the differences in the force-time patterns of the different touches. It should be remembered, however, that in the present model, the string is assumed to be ideally rigid. This assumption may eliminate the complex interaction between the vibratory motion of the hammer-shank system and the string. Even if the shank deformation is very small ($\ll$0.5mm), a slight difference in the deformation pattern (due to the difference of the touch) might cause an audible difference in the excitation of the string.

IV. CONCLUSIONS

The effect of the shank of the piano hammer was investigated using a mathematical model which consists of fourteen (including hammer) elements rigidly connected to each other.

At one end, the shank was pivot-supported, and at the other end a mass-spring system with a nonlinear spring coefficient was attached to simulate the function of the hammer. The Myklestad method was modified and used to analyze the transient motion of the hammer-shank system during the contact period with an ideally rigid string. The force applied by the hammer to the string and the deformation of the shank were evaluated as a function of time to see the effect of the shank.

With a normal shank stiffness and mass, the maximum deformation of the shank is significant (= 0.75 mm) during the contact period for the case of a hard-hit key. If the shank is made stiff enough so that the shank is not deformed during the contact period, the force-time pattern becomes wider since a larger portion of the shank mass is added to the hammer mass making the effective mass of the hammer larger.

If we assume that the shank is initially deformed due to the large acceleration during the upward motion of the hammer-shank system, the force-time pattern can be different for positive and negative initial

deformations of the shank. However, it was found from the experiment that the actual initial deformation of the shank must be much smaller than the value used for the calculation (0.5 mm).

The attempt to explain the difference of the touch as the result of the shank deformation was not successful, but the finding that the shank is deformed significantly during the contact period is important. A deformation of the shank by 0.75 mm causes the horizontal motion of the hammer head by approximately the same amount. This seems significant considering that the vertical deformation of the hammer is in the same order (for hammers of low notes). The rubbing of the string by the hammer head during the contact period, as well as the vibratory motion of the shank during this period, may cause some audible effect on the vibration of the string.

The analysis of the transient motion of a model which takes into account the finite impedance of the string and the rotary inertia of the hammer is left as future work.

REFERENCES

[1] H.L.F. Helmholtz, "Sensation of Tone", (Dover Publications, Inc., New York, 1954)

[2] W. Kaufmann, "Uber die Bewegungen geschlagener Klaviersaiten", Ann. Phys., 54, 674-72 (1885)

[3] W.H. George, "On the Helmholtz Theories of the Struck String", Phil. Mag., 6(47), 591-602 (1924)

[4] S. Bhargava and R. N. Ghosh, "Elastic Impact of Pianoforte Hammer", Phil Mag., 6(47), 1141-1149 (1924)

[5] W.H. George, "On the Helmholtz Theories of the Struck String, Part II, Experimental", Phil. Mag., 6(48), 34-49 (1924)

[6] S. Bharagave and R.N. Ghosh, "On the Elastic Impact of the Pianoforte Hammer, Part II", Phil. Mag., 6(49), 121-129 (1925)

[7] W.H. George and H.E. Beckett, "The Energy of the Struck String", Proc. Roy. Soc., A114 111-139 (1927)

[8] W.H. George and H.E. Beckett, "The Energy of the Struck String", Proc. Roy. Soc., A116, 115-140 (1927)

[9] D. Banerji and R. Ganguli, "the Duration of Contact Between the Pianoforte String and a Hard Hammer", Phil. Mag., 7(7) 345-352, (1929)

[10] M. Ghosh, "On the Hertzian Impact of an Elastic Hammer on a Damped Pianoforte String", Phil. Mag., 7(17), 521-544 (1934)

[11] N. Davy. J.H. Littlewood, and M. McCaig, "The Force-Time Law Governing the Impact of a Hammer on a Stretched String", Phil. Mag., 7(27), 133-143 (1939)

[12] K.K. Deb, "Dynamics of the Pianoforte String and Hammer", J. Sound & Vib., 20(1), 1-7 (1972)

[13] I. Nakamura, "The Vibration of a Struck String — Acoustical Research on the Piano, Part I", J. Acoust. Soc. Jpn., 36(10) 504-512 (1980)

[14] N.O. Myklestad Fundamentals of Vibration Analysis, (McGraw-Hill, New York. 1956)

[15] R.K. Vierck, Vibration Analysis (Thomas Crowell Company, Harper & Row, Publishers New York, 1979)

Table I Dimensions of the shank elements

Element N Number j	Width a(cm)	Height b(cm)	Radius r(cm)	Length ℓ(cm)	Mass m(gram)	Area Moment of Inertia I(cm^4)
						10^{-2}
1	0.54	0.655	—	0.8	0.05	1.3
2	1.2	0.655	—	1.7	1.21*	2.8
3	0.71	0.655	—	1.1	0.66	1.7
4	0.71	0.655	—	1.3	0.40	1.7
5	—	—	0.65	1.0	0.335	0.88
6	—	—	0.645	1.0	0.24	0.85
7	—	—	0.645	1.0	0.24	0.85
8	—	—	0.63	1.0	0.23	0.77
9	—	—	0.61	1.0	0.215	0.68
10	—	—	0.59	1.0	0.20	0.59
11	—	—	0.57	1.0	0.19	0.52
12	—	—	0.54	0.5	0.175	0.42
13	—	—	0.53	0.4	0.16	0.39

* Additional mass of the knuckle is included.

Table II Standard values of the system parameters

Hammer Mass	M_h	10 gram
Hammer Stiffness	S_h	$1.8 \times 10^{10} y_h^3$ dyne/cm
Hammer Velocity	V_h	3 m/sec
Young's Modulus of Shank	E_s	10^{11} dyne/cm^2
Density of Shank	ρ_s	0.72 gram/cm^2
Initial Shank Deformation		Zero

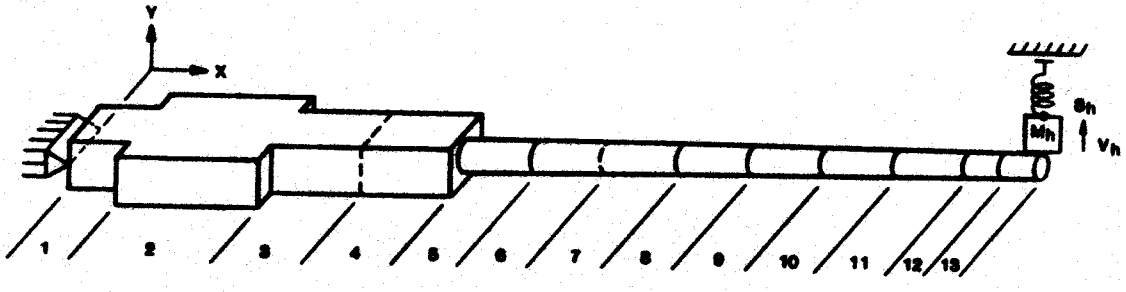

FIG. 1 HAMMER-SHANK MODEL

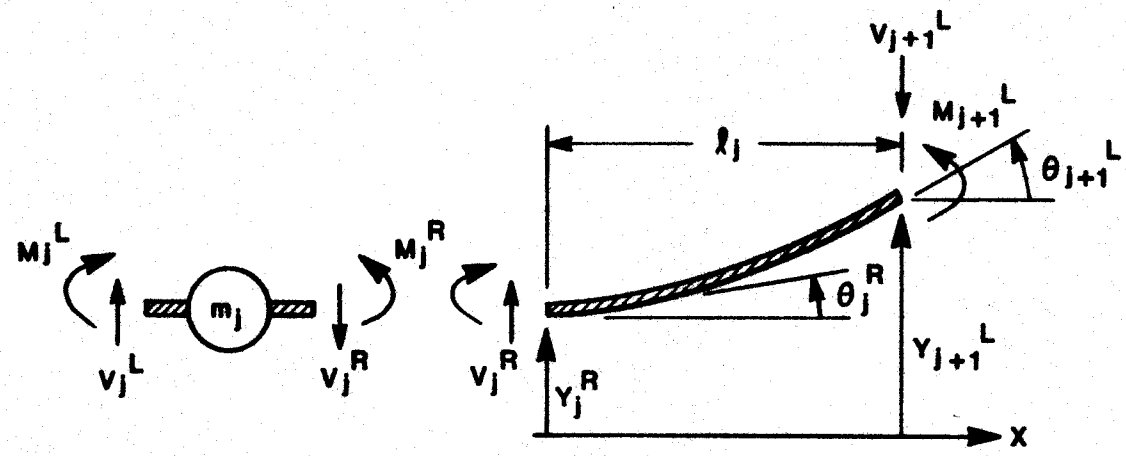

FIG. 2 LUMPED MASS AND A MASSLESS ELASTIC BEAM AS A MATHEMATICAL MODEL OF THE ELEMENT SHOWN IN FIG. 1

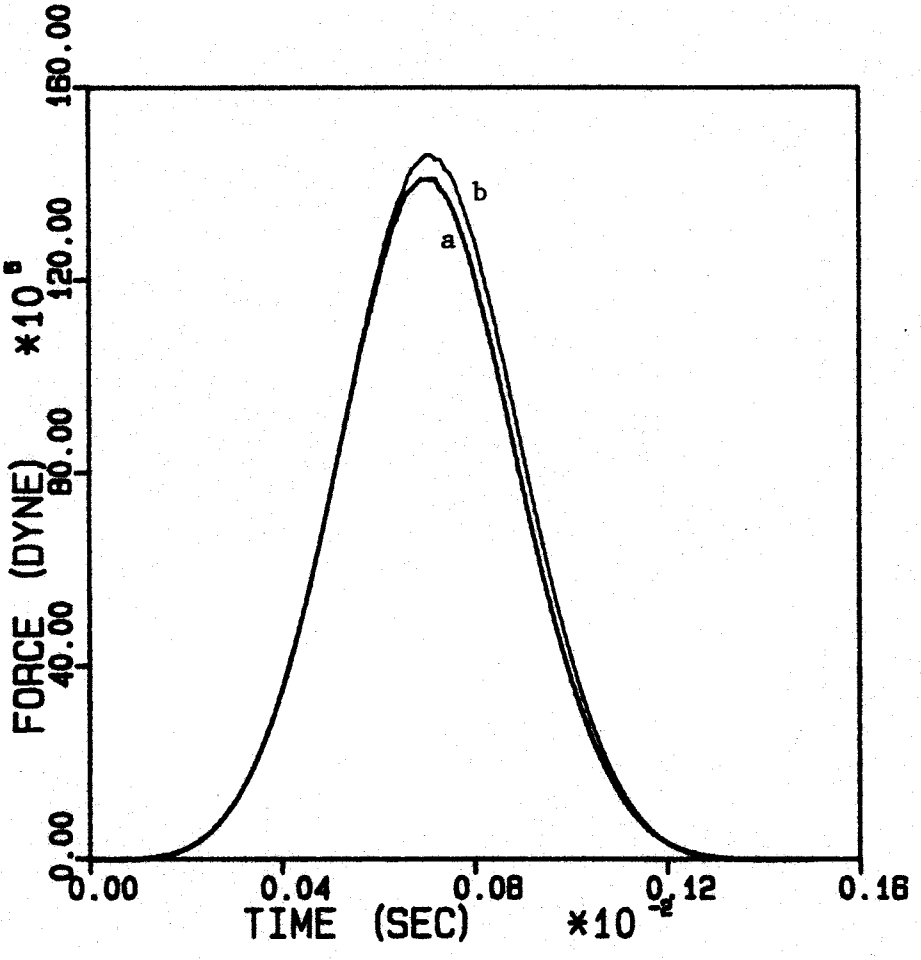

FIG. 3 FORCE-TIME PATTERNS OF THE SYSTEM WITH STANDARD PARAMETERS (a) AND WITH $E_S=10^{12}$ DYNE/CM^2 (b).

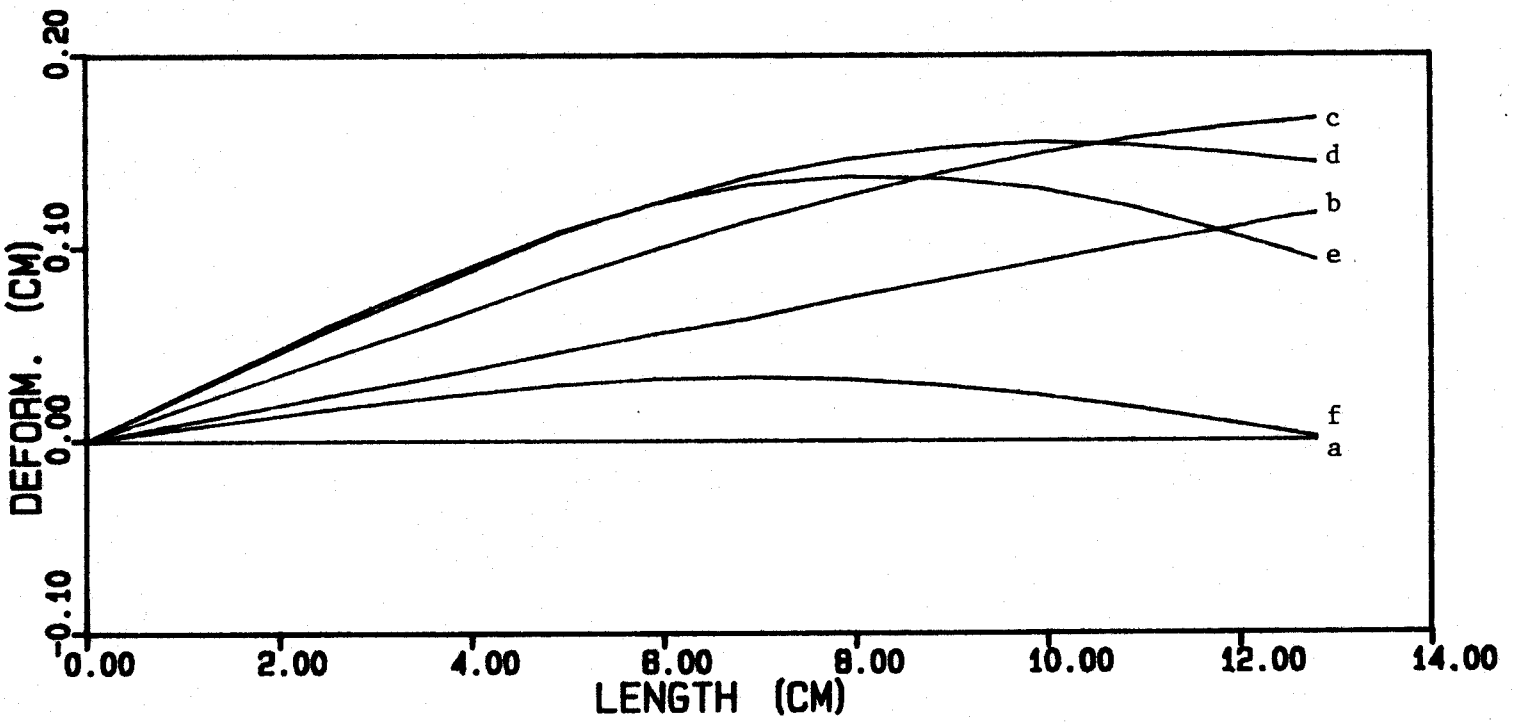

FIG. 4 DEFORMATIONS OF THE SHANK OF THE SYSTEM WITH STANDARD PARAMETERS AT t = 0(a), 0.4(b), 0.71(c), 0.9(d), 1.1(e), AND 1.4 MSEC(f), RESPECTIVELY

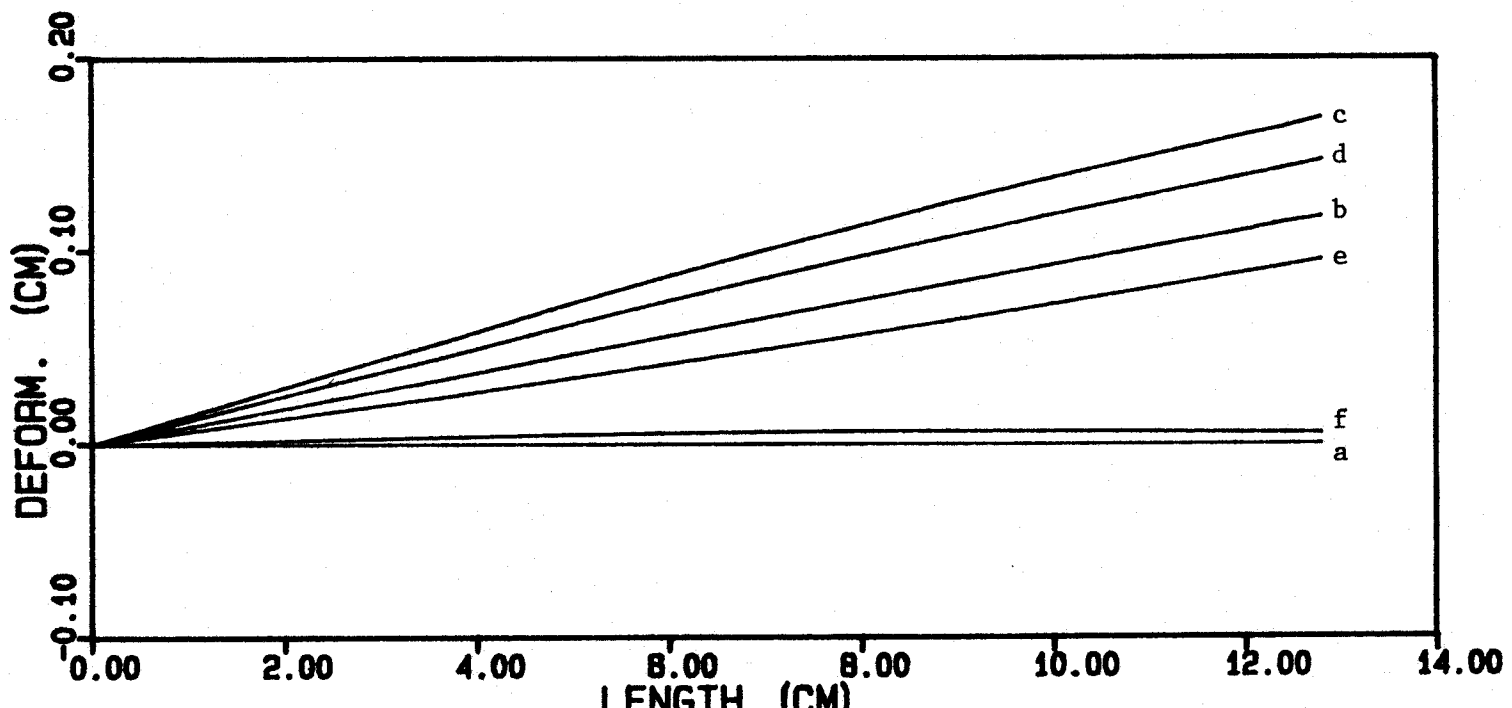

FIG. 5 DEFORMATIONS OF THE SHANK OF THE SYSTEM WITH $E_S = 10^{12}$ DYNE/CM^2 (OTHER PARAMETERS ARE STANDARD) AT t = 0(a), 0.4(b), 0.7(c), 0.9(d), 1.1(e), AND 1.4 MSEC(f), RESPECTIVELY

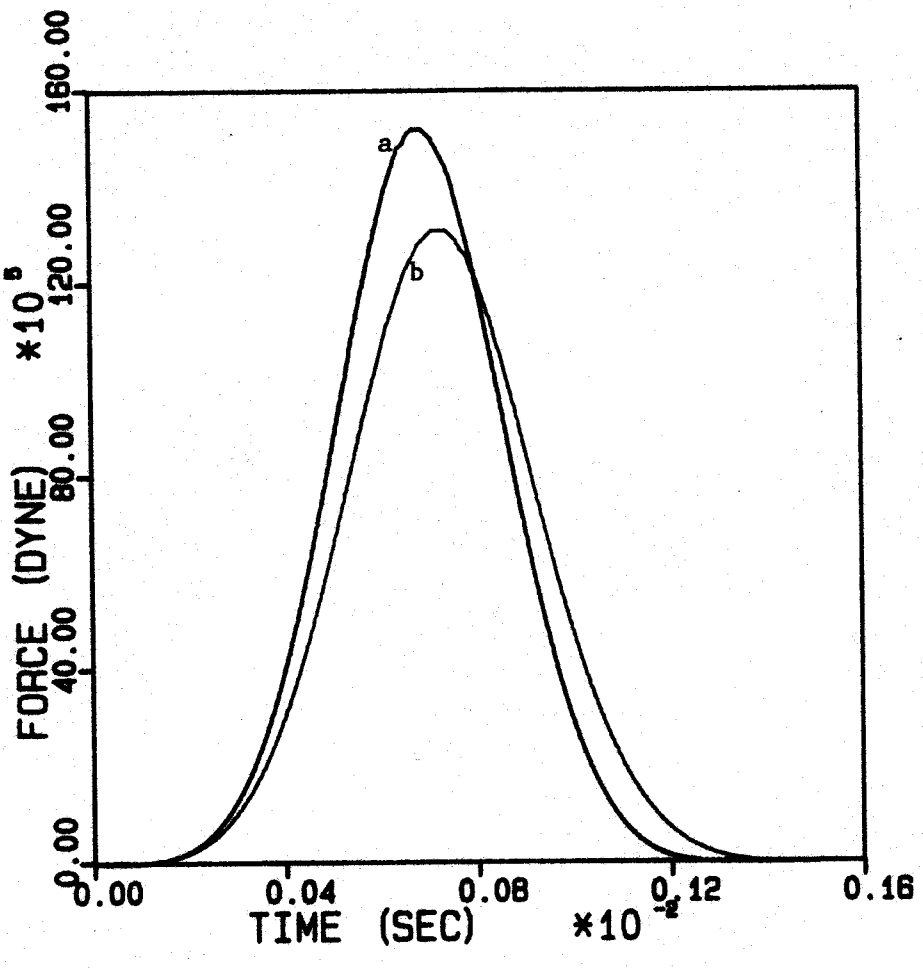

FIG. 6 FORCE-TIME PATTERNS OF THE SYSTEM WITH POSITIVE (a) AND NEGATIVE (b) INITIAL DEFORMATIONS.

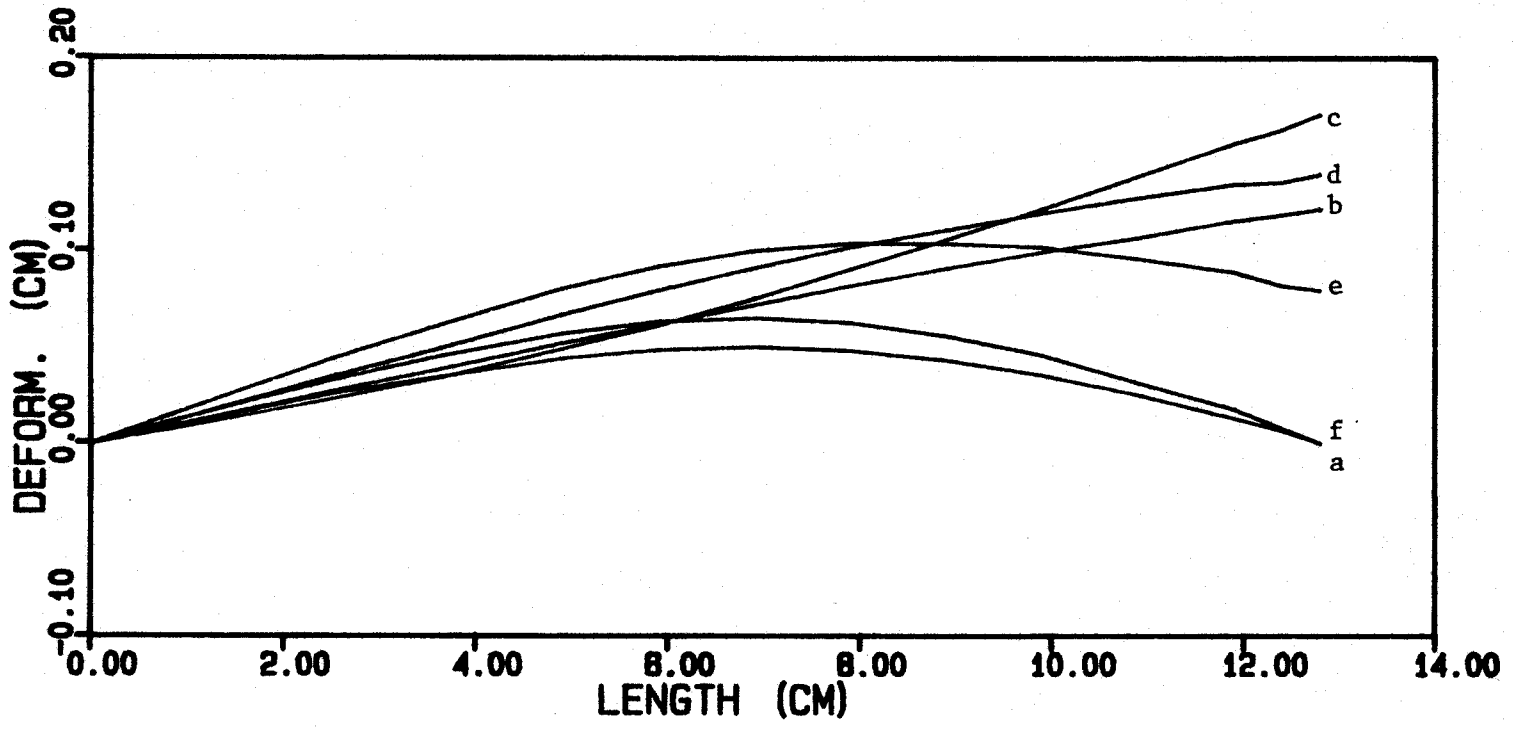

FIG. 7 DEFORMATIONS OF THE SHANK OF THE SYSTEM WITH POSITIVE INITIAL DEFORMATION AT t = 0(a), 0.4(b), 0.7(c), 0.9(d), 1.1(e), AND 1.4 MSEC(f) RESPECTIVELY.

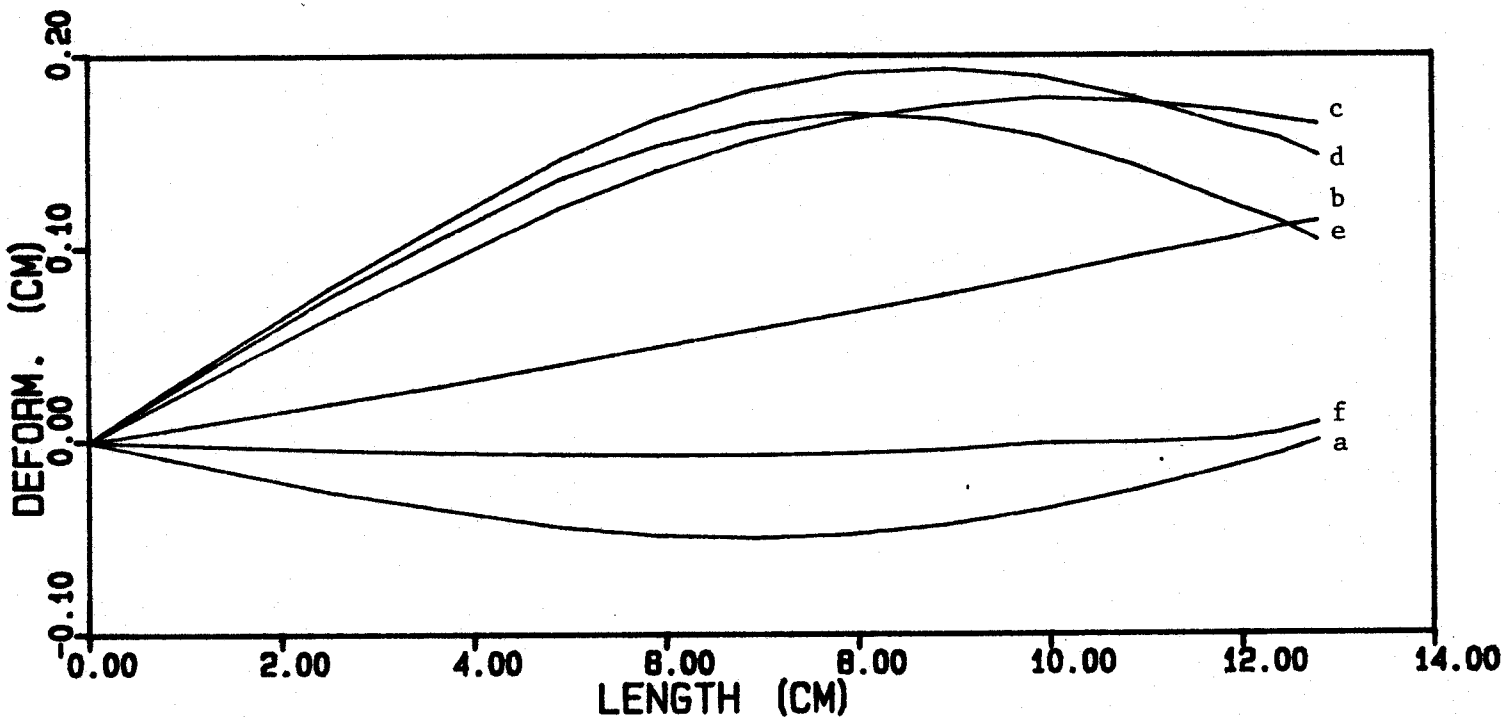

FIG. 8 DEFORMATIONS OF THE SHANK OF THE SYSTEM WITH THE NEGATIVE INITIAL DEFORMATION AT t = 0(a), 0.4(b), 0.7(c), 0.9(d), 1.1(e), AND 1.4 MSEC(f), RESPECTIVELY.

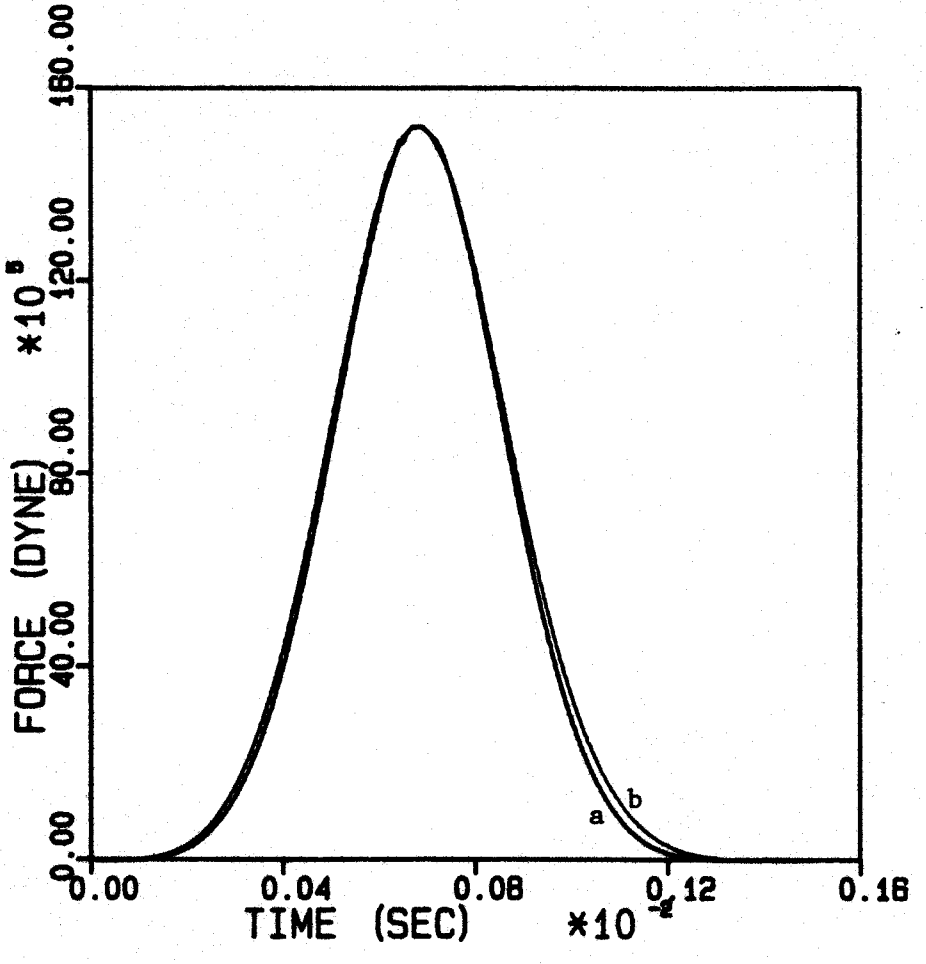

FIG. 9 FORCE-TIME PATTERNS OF THE SYSTEM WITH THE POSITIVE INITIAL DEFORMATION AND V_h =3M/SEC (a) AND THE SYSTEM WITH THE NEGATIVE INITIAL DEFORMATION AND V_h =3.29M/SEC (b).

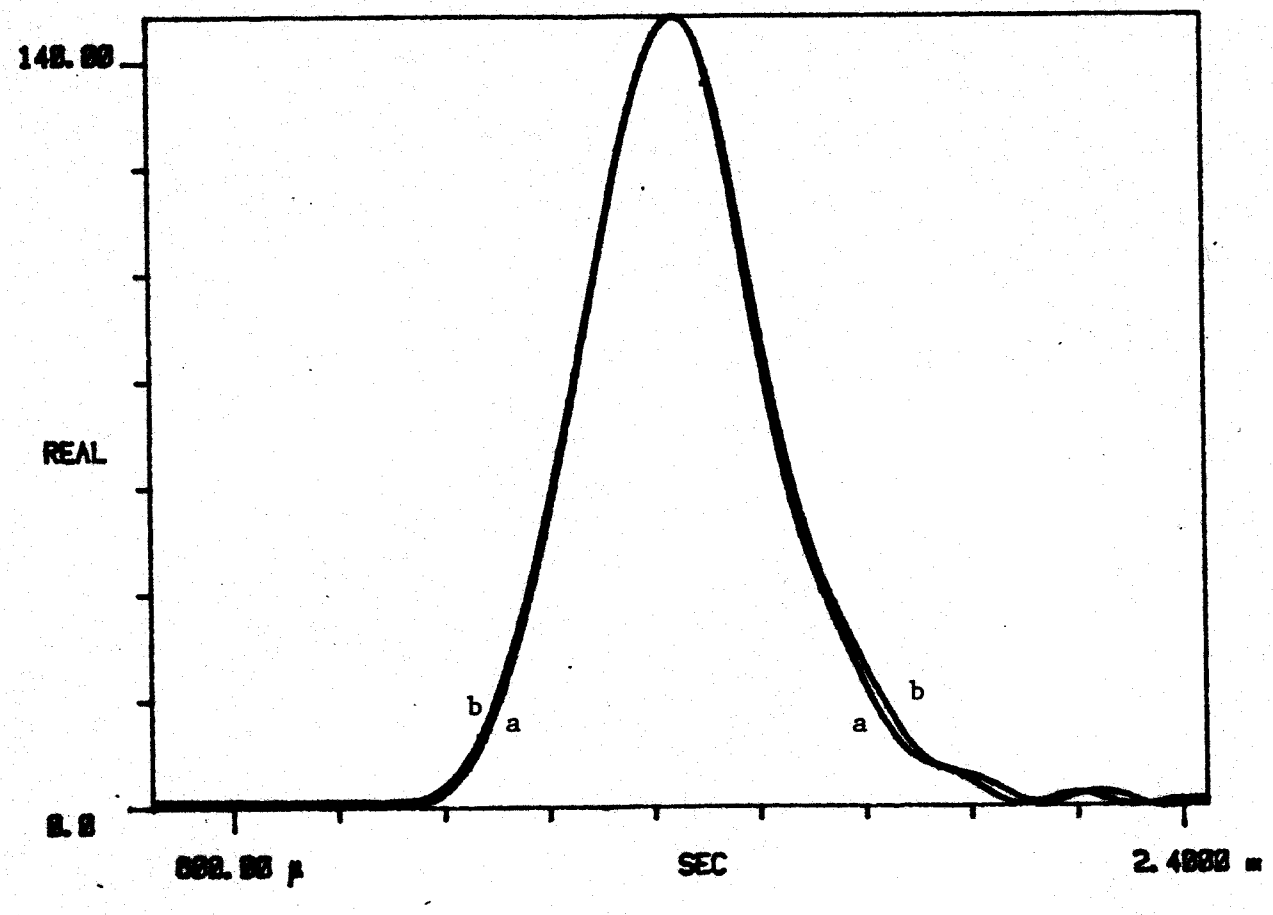

FIG. 10 MEASURED FORCE-TIME PATTERNS OF A HAMMER-SHANK SYSTEM WITH A WOOD SHANK (a) AND A CARBON-FIBER TUBE SHANK (b).